Miner Petrol (2016) 110:917–926
DOI 10.1007/s00710-016-0454-2

ORIGINAL PAPER

# Bunnoite, a new hydrous manganese aluminosilicate from Kamo Mountain, Kochi prefecture, Japan

**Daisuke Nishio-Hamane**[1] · **Koichi Momma**[2] · **Ritsuro Miyawaki**[2] · **Tetsuo Minakawa**[3]

Received: 30 March 2016 / Accepted: 12 July 2016 / Published online: 27 July 2016


**Abstract** A new mineral, bunnoite, originating from Kamo Mountain in Ino, Kochi Prefecture, Japan, has been identified. Bunnoite occurs as veins and lenses in hematite-rich ferro-manganese ore, is dull green in color, and forms foliated subhedral crystals up to 0.5 mm in length. Its hardness is 5½ on the Mohs scale and its calculated density is 3.63 g cm$^{-3}$. The mineral is optically biaxial (+), with $\alpha$ = 1.709(1), $\beta$ = 1.713(1), $\gamma$ = 1.727(1) (white light), $2V_{meas}$ = 54° and $2V_{calc}$ = 57°. The empirical formula of bunnoite is $(Mn^{2+}_{5.36}Mg_{0.27}Fe^{2+}_{0.25}Fe^{3+}_{0.11})_{\Sigma 6.00}(Al_{0.60}Fe^{3+}_{0.40})_{\Sigma 1.00}(Si_{5.89}Al_{0.11})_{\Sigma 6.00}O_{18}(OH)_3$, and its simplified ideal formula is written as $Mn^{2+}_6AlSi_6O_{18}(OH)_3$. The mineral is triclinic $P\bar{1}$, and the unit cell parameters refined from powder X-ray diffraction data are $a$ = 7.521(5) Å, $b$ = 10.008(8) Å, $c$ = 12.048(2) Å, $\alpha$ = 70.46(5)°, $\beta$ = 84.05(6)°, $\gamma$ = 68.31(6)° and $V$ = 793.9(9) Å$^3$. The crystal structure of bunnoite has been solved by the charge flipping method in conjunction with single-crystal X-ray diffraction data and refined to $R1$ = 3.3 %. Bunnoite was found to have a layered structure with alternating tetrahedral and octahedral sheets parallel to the (1 11). The silicate tetrahedra form sorosilicate $[Si_6O_{18}(OH)]$ clusters in the tetrahedral sheets, while the octahedra share edges to form continuous strips linked by $[Mn_2O_8]$ dimers in the octahedral sheets. This mineral is classified as 9.BH according to the Nickel-Strunz system and has been named in honor of the Japanese mineralogist Michiaki Bunno (b. 1942).

**Keywords** Bunnoite · New mineral · Hydrous manganese aluminosilicate · Ferro-manganese deposit · Crystal structure · Kochi prefecture

## Introduction

Various small scale iron-manganese deposits are distributed around the Ino district within Kochi Prefecture, Shikoku, Japan. During a mineralogical survey of these deposits, one of the authors (T. M.) collected hematite-rich ore from the unnamed iron-manganese deposits located at Kamo Mountain. These ore samples included a foliated mineral dull green in color, and initial mineralogical investigations revealed that this material was a hydrous manganese aluminosilicate. To date, six hydrous manganese aluminosilicates have been accepted as valid mineral species: akatoreite $Mn^{2+}_9Al_2Si_8O_{24}(OH)_8$, carpholite $Mn^{2+}Al_2Si_2O_6(OH)_4$, davreuxite $Mn^{2+}Al_6Si_4O_{17}(OH)_2$, kellyite $(Mn^{2+},Mg,Al)_3(Si,Al)_2O_5(OH)_4$, ottrélite $Mn^{2+}Al_2O(SiO_4)(OH)_2$, and pennantite $(Mn^{2+}Al)_6(Si,Al)_4O_{10}(OH)_8$ (e.g. Smith et al. 1946; Read and Reay 1971; Naumova et al. 1974; Peacor et al. 1974; Fransolet 1978; Fransolet et al. 1984). Since the chemical composition of the unidentified mineral from Kamo Mountain was similar to that of akatoreite, this mineral was initially reported to be akatoreite (Minakawa 2000). However,

Editorial handling: N. V. Chukanov

**Electronic supplementary material** The online version of this article (doi:10.1007/s00710-016-0454-2) contains supplementary material, which is available to authorized users.

✉ Daisuke Nishio-Hamane
hamane@issp.u-tokyo.ac.jp

[1] Institute for Solid State Physics, The University of Tokyo, Kashiwa, Chiba 277–8581, Japan

[2] Department of Geology and Paleontology, National Museum of Nature and Science, Tsukuba 305–0005, Japan

[3] Department of Earth Science, Faculty of Science, Ehime University, Matsuyama, Ehime 790–8577, Japan

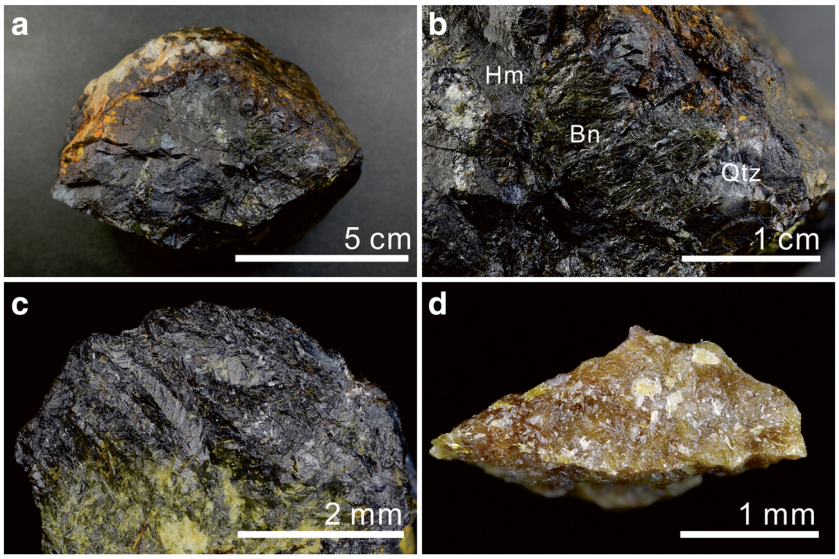


**Fig. 1** Photographic images of bunnoite and akatoreite: (**a**) complete image of the bunnoite-bearing hematite-rich ore, (**b**) a close-up image of the same specimen, (**c**) a bunnoite aggregate, and (**d**) an akatoreite aggregate from eastern Otago, New Zealand. Bn, bunnoite; Hm, hematite; Qtz, quartz

the appearance of this mineral is different from those of akatoreite specimens found in other localities. Recent detailed examinations, including crystal structure determination, have since shown that this is in fact a new mineral species distinct from akatoreite.

This new mineral has been named bunnoite in honor of Michiaki Bunno (b. 1942), a scientist specializing in descriptive mineralogy who was chief curator for the Geological Museum of the Geological Survey of Japan, and who put together the Museum's archive of mineral specimens. After retirement, Dr. Bunno has worked to retrieve forgotten samples from storage at many universities. His contributions to the field also include the discovery of new minerals: potassic-ferro-sadanagaite, potassic-sadanagaite, proto-ferro-anthophyllite, proto-ferro-suenoite, wadalite, and sadanagaite. In light of all this, it is evident that Dr. Bunno's work has certainly contributed to mineralogy. Both the new mineral and its name have been approved by the International Mineralogical Association, Commission on New Minerals, Nomenclature and Classification (no. 2014–054). The type specimen has been deposited in the collections of the National Museum of Nature and Science, Japan, specimen number NSM–M44106.

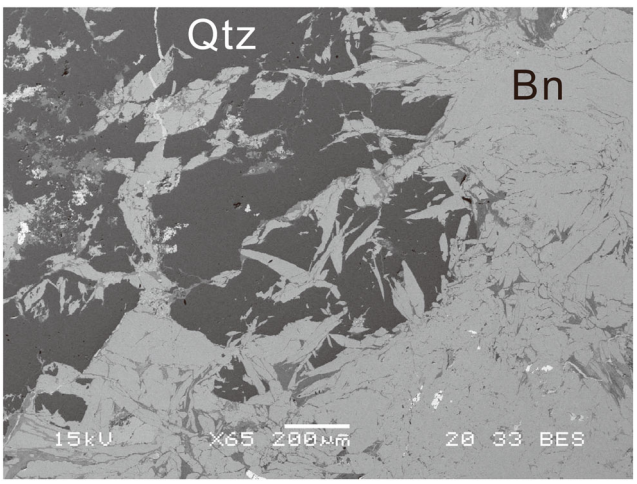


**Fig. 2** Back scattered electron image of bunnoite. Bunnoite consists of foliated subhedral crystals in quartz vein and a small amount of the ore minerals shown as different contrast fills the crevice of bunnoite crystal. Bn, bunnoite; Qtz, quartz

## Occurrence and general appearance

The Ino district is located in the central part of Kochi Prefecture, Shikoku Island, Japan. The geology of this district is primarily composed of the metamorphic complexes of the Kurosegawa tectonic zone and the accretionary complexes of the Chichibu terrane, which are distributed from east to west. The main constituents of the former geological unit are divided into the Terano, older Ino, and younger Ino metamorphic complexes (e.g., Wakita et al. 2006). The younger Ino metamorphic complex consists mainly of mafic and pelitic schist in association with small quantities of psammitic schist, limestone and chert. These were generated by pumpellyite-

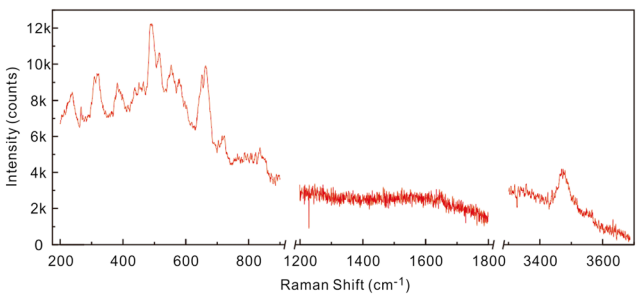


**Fig. 3** Raman spectra of bunnoite

**Table 1** Chemical composition of bunnoite and of akatoreite for comparison

| | Bunnoite | | Akatoreite | |
|---|---|---|---|---|
| Constituent | Mean ($n$ = 5) | Ideal | Mean ($n$ = 5) | Ideal |
| $SiO_2$ | 40.44 (39.60–41.40) | 41.72 | 36.77 (36.71–36.86) | 37.17 |
| $Al_2O_3$ | 4.15 (3.30–5.16) | 5.90 | 7.61 (7.28–7.88) | 7.88 |
| $Fe_2O_3$ | 6.98 (6.04–8.36) | – | 1.61 (1.28–1.78) | – |
| MnO | 43.50 (42.10–44.49) | 49.25 | 46.94 (46.29–47.51) | 49.37 |
| MgO | 1.26 (1.11–1.44) | – | 0.45 (0.35–0.63) | – |
| CaO | – | – | 0.20 (0.12–0.25) | – |
| Total | 96.33 | 96.87 | 93.60 | 94.42 |
| *FeO | 2.05 | – | 1.10 | – |
| *$Fe_2O_3$ | 4.70 | – | 0.39 | – |
| *$H_2O$ | 3.09 | 3.13 | 5.52 | 5.57 |
| Total | 99.19 | 100 | 98.80 | 100 |
| Basis of | O = 18, OH = 3 | | O = 24, OH = 8 | |
| Si | 5.89 | 6 | 7.99 | 8 |
| Al | 0.11 | – | 0.01 | – |
| Σ | 6.00 | | 8.00 | |
| Al | 0.60 | 1 | 1.94 | 2 |
| $Fe^{3+}$ | 0.40 | – | 0.06 | – |
| Σ | 1.00 | | 2.00 | |
| $Mn^{2+}$ | 5.36 | 6 | 8.65 | 9 |
| $Fe^{2+}$ | 0.25 | – | 0.20 | – |
| $Fe^{3+}$ | 0.11 | – | 0.01 | – |
| Mg | 0.27 | – | 0.15 | – |
| Ca | – | – | 0.00 | – |
| Σ | 6.00 | | 9.00 | |

*calculated from stoichiometry

**Table 2** X-ray powder diffraction data for bunnoite

| $h\ k\ l$ | $I/I_0$ | $I_{calc.}$ | $d_{obs.}$ (Å) | $d_{calc.}$ (Å) |
|---|---|---|---|---|
| 001 | 3 | 2 | 11.3380 | 11.3505 |
| 010 | 2 | 4 | 8.7900 | 8.8086 |
| 011 | 4 | 12 | 8.3862 | 8.3804 |
| 100 | 2 | 3 | 6.9703 | 6.9864 |
| 101 | 4 | 8 | 5.8824 | 5.8900 |
| 012 | 7 | 6 | 5.6972 | 5.6693 |
| 121, 1–10 | 8 | 9, 1 | 4.7375 | 4.7495, 4.71477 |
| 1–1-1 | 54 | 50 | 4.6710 | 4.6746 |
| 122 | 4 | 2 | 4.2498 | 4.2498 |
| 01–2, 022 | 8 | 7, 2 | 4.2006 | 4.1974, 4.1902 |
| 11–2 | 5 | 4 | 3.9392 | 3.9380 |
| 12–1 | 2 | 1 | 3.8034 | 3.8118 |
| 02–1 | 2 | 3 | 3.7198 | 3.7233 |
| 113 | 2 | 2 | 3.6797 | 3.6733 |
| 023, 221 | 37 | 46, 4 | 3.4681 | 3.4723, 3.4680 |
| 1–2-1, 1–12 | 92 | 6, 34 | 3.3339 | 3.3403, 3.3332 |
| 201 | 89 | 43 | 3.3197 | 3.3175 |
| 132 | 28 | 50 | 3.2385 | 3.2381 |
| 1–2-2 | 15 | 22 | 3.1727 | 3.1700 |
| 01–3 | 4 | 2 | 3.1337 | 3.1314 |
| 02–2, 032 | 17 | 2, 16 | 3.0356 | 3.0395, 3.0349 |
| 133, 1–21 | 11 | 11, 8 | 2.9359 | 2.9421 |
| 2–10 | 23 | 17 | 2.9109 | 2.9103 |
| 124, 004, 1–2-3 | 26 | 2, 3, 22 | 2.8338 | 2.8396, 2.8376, 2.8292 |
| 1–13 | 70 | 41 | 2.7119 | 2.7136 |
| 1–1-4, 22–2 | 100 | 7, 100 | 2.6572 | 2.6609, 2.6589 |
| 233 | 43 | 28 | 2.6359 | 2.6363 |
| 104 | 40 | 21 | 2.6085 | 2.6084 |
| 1–22, 23–1, 12–3, 203 | 25 | 2, 3, 2, 1 | 2.5454 | 2.5557, 2.5473, 2.5379, 2.5366 |
| 310, 321, 01–4, 141, 034 | 17 | 8, 2, 1, 4, 1 | 2.4758 | 2.4811, 2.4790, 2.4774, 2.4773, 2.4750 |
| 311 | 5 | 8 | 2.4581 | 2.458 |
| 015, 143, 322 | 13 | 8, 1, 5 | 2.3886 | 2.3913, 2.3912, 2.3896 |
| 241 | 14 | 2 | 2.3700 | 2.3667 |
| 30–1 | 6 | 2 | 2.2917 | 2.2916 |
| 1–1-5, 144 | 60 | 5, 46 | 2.2158 | 2.2135, 2.2132 |
| 040 | 40 | 24 | 2.2026 | 2.2022 |
| 2–13, 204 | 48 | 35, 1 | 2.1799 | 2.1790, 2.1783 |

$a$ = 7.521(5), $b$ = 10.008(8), $c$ = 12.048(7) Å, $\alpha$ = 70.46(5), $\beta$ = 84.05(6), $\gamma$ = 68.31(6)°, $V$ = 793.8(9)Å$^3$

actinolite subfacies metamorphism and their K-Ar radiometric ages range from Triassic to Jurassic. A number of small-scale mines targeting iron-manganese deposits once operated in the younger Ino metamorphic complex. These deposits were formed from iron- and manganese-rich marine sediments during low-grade metamorphism.

Kamo Mountain (33°33′24.4″ N 133°25′29.4″ E) is located to the north of Ino town, and its geology corresponds to the younger Ino metamorphic complex. The rocks in this region consist primarily of pelitic schist with smaller amounts of chert, and the K-Ar radiometric age of the phengite in the pelitic schist from the west slope of the mountain is 161 Ma (e.g. Wakita et al. 2006). Iron-manganese deposits have also been found on Kamo Mountain, although the name of mines and deposits has not been recorded. Samples including bunnoite were collected from one of these deposits, situated on the south slope of the mountain. These rock specimens have a black coloration and consist mainly of hematite in association with stilpnomelane, rhodonite, piemontite and quartz. Bunnoite is present as veins and lenses in this hematite-rich ore (Fig. 1). Bunnoite consists of foliated subhedral crystals in a quartz vein and a small amount of the above-listed ore minerals fills the crevice of bunnoite crystals (Fig. 2.). The bunnoite veins randomly cross the ore, and were most likely formed by hydrothermal activity at a later stage during metamorphism.

**Table 3** Data collection and details of the structural refinement for bunnoite

| Temperature | 296(2) K |
|---|---|
| Radiation | Mo$K\alpha$ |
| Crystal size | 0.07 × 0.05 × 0.02 mm |
| Space Group | *P*-1 |
| Unit cell dimensions | $a$ = 7.505(3), $b$ = 9.987(3), $c$ = 12.060(4) Å |
| | $\alpha$ = 70.526(5), $\beta$ = 84.224(7), $\gamma$ = 68.460(4)° |
| Volume | $V$ = 792.4(5) Å$^3$ |
| $Z$ | 2 |
| $F$(000) | 839 |
| Absorption coefficient $m$(Mo$K\alpha$) | 5.44 mm$^{-1}$ |
| Diffractometer | R-AXIS RAPID II |
| Voltage, Current | 50 kV, 24 mA |
| 2$\theta$max | 59.0° |
| No. of Reflections Measured | 8869 |
| Independent reflections | 4386 |
| Structure Solution | Superflip (Palatinus and Chapuis 2007) |
| Refinement | Full-matrix least-squares on $F^2$ |
| Function Minimized | $\Sigma w(F_o^2 - F_c^2)^2$ |
| Least Squares Weights | $w = 1/ [\sigma^2(F_o^2) + (0.0275P)^2 + 1.5087P]$ |
| | where $P = (F_o^2 + 2F_c^2)/3$ |
| Residuals: $R1$ ($I > 2\sigma(I)$) | 0.0334 |
| Residuals: $R$ (All reflections) | 0.0390 |
| Residuals: $wR2$ (All reflections) | 0.0780 |
| Goodness of Fit Indicator | 1.132 |
| Largest diff. Peak and hole | 1.04 e/Å$^3$ and −0.78 e/Å$^3$ |

## Physical and optical properties

The large crystal of bunnoite is dull green in color and consists of foliated subhedral crystals up to 0.5 mm in length shown as (upper part in Fig. 1c), while aggregates of fine-grained crystal show yellowish green colour (lower part in Fig. 1c). It has a vitreous luster and small crystals are transparent, while larger crystal blocks are translucent. Its streak is also dull green and its Mohs hardness is 5½. The mineral is brittle and it exhibits perfect cleavage along the {012} plane. Its fracture is uneven. The density, as calculated based on the empirical formula and powder unit cell data, is 3.63 g cm$^{-3}$. The experimental density has not yet been measured accurately owing to the presence of inclusions. Bunnoite is optically biaxial (+), with $\alpha$ = 1.709(1), $\beta$ = 1.713(1), $\gamma$ = 1.727(1) (white light), $2V_{meas}$ = 54° and $2V_{calc}$ = 57°. Pleochroism varies from pale greenish yellow to brownish yellow.

## Raman spectroscopy

Raman spectroscopic analysis was performed with a HORIBA HR320 spectrometer using a 100 mW, 514.5 nm argon laser. Raman shifts were calibrated using silicon, the spectra were obtained by 5 s measurements with 200 times integration, and the resulting spectra are shown in Fig. 3. Although the spectral signals were weak, several peaks could be distinguished. The peaks in the region below 900 cm$^{-1}$ are thought to be derived from metal–anion stretching vibrations, while those in the region of 3400–3600 cm$^{-1}$ are attributed to O–H stretching. No peaks were found between 1200 and 1800 cm$^{-1}$ in the spectra of bunnoite, indicating the absence of H–O–H bending vibrations.

## Chemical composition

Table 1 summarizes the chemical analysis of bunnoite. Chemical analyses of this mineral were carried out using a JEOL JSM–5600 electron microprobe (EDS mode, 15 kV, 0.4 nA, 2 μm beam diameter), and ZAF method was used for data correction. The live time was set at 90 s, and the peak count and position were calibrated using cobalt metal. The detection limit for EDS method is commonly ~0.1 wt%, and the detected elements exceeding this limit were Si, Al, Fe, Mn, and Mg for bunnoite. The probe standards used were silicon

**Table 4** Refined atom positions and isotropic or equivalent isotropic displacement parameters (Å$^2$) for bunnoite

| | *x* | *y* | *z* | $U_{iso}$*/$U_{eq}$ | Occ. |
|---|---|---|---|---|---|
| Mn1 | 0.01588 (6) | 0.12574 (5) | 0.39091 (4) | 0.01124 (10) | 1.0Mn |
| Mn2 | 0.17099 (6) | 0.38859 (5) | 0.30940 (4) | 0.01005 (10) | 1.0Mn |
| Mn3 | 0.61247 (6) | 0.11534 (5) | 0.99505 (4) | 0.00963 (9) | 1.0Mn |
| Mn4 | 0.18019 (6) | 0.63940 (5) | 0.05630 (4) | 0.01127 (10) | 1.0Mn |
| Mn5 | 0.62615 (6) | 0.85906 (5) | 0.24631 (4) | 0.00911 (11) | 0.930(2)Mn + 0.070(2)Mg |
| Mn6 | 0.40124 (7) | 0.63130 (5) | 0.26601 (4) | 0.00813 (12) | 0.440(2)Mn + 0.36Fe + 0.200(2)Mg |
| Al7 | 0.61597 (8) | 0.61128 (6) | 0.48539 (5) | 0.00968 (12) | 0.60Al + 0.40Fe |
| Si1 | 0.60822 (11) | 0.36260 (8) | 0.15505 (7) | 0.00725 (14) | 0.98Si + 0.02Al |
| Si2 | 0.20637 (10) | 0.15031 (8) | 0.13716 (7) | 0.00658 (14) | 0.98Si + 0.02Al |
| Si3 | 0.00306 (11) | 0.69003 (8) | 0.41927 (7) | 0.00775 (14) | 0.98Si + 0.02Al |
| Si4 | 0.00900 (11) | 0.91873 (8) | 0.17830 (7) | 0.00730 (14) | 0.98Si + 0.02Al |
| Si5 | 0.79772 (11) | 0.60492 (8) | 0.10555 (7) | 0.00690 (14) | 0.98Si + 0.02Al |
| Si6 | 0.61641 (11) | 0.14091 (8) | 0.39326 (7) | 0.00801 (15) | 0.98Si + 0.02Al |
| O1 | 0.7893 (3) | 0.0608 (2) | 0.48850 (18) | 0.0113 (4) | |
| O2 | 0.9895 (3) | 0.3055 (2) | 0.44853 (17) | 0.0096 (4) | |
| O3 | 0.5918 (3) | 0.4704 (2) | 0.41375 (19) | 0.0114 (4) | |
| O4 | 0.1927 (3) | 0.8010 (2) | 0.13486 (18) | 0.0096 (4) | |
| O5 | 0.4016 (3) | 0.4696 (2) | 0.18526 (18) | 0.0097 (4) | |
| O6 | 0.4233 (3) | 0.2595 (2) | 0.42465 (17) | 0.0095 (4) | |
| O7 | 0.8116 (3) | 0.9385 (2) | 0.12549 (18) | 0.0115 (4) | |
| O8 | 0.8082 (3) | 0.6724 (2) | 0.39100 (18) | 0.0107 (4) | |
| O9 | −0.0066 (3) | 0.5546 (2) | 0.17558 (18) | 0.0113 (4) | |
| O10 | 0.4062 (3) | 0.0323 (2) | 0.11161 (18) | 0.0099 (4) | |
| O11 | 0.2019 (3) | 0.1843 (2) | 0.25992 (17) | 0.0105 (4) | |
| O12 | 0.6074 (3) | 0.7115 (2) | 0.15076 (18) | 0.0094 (4) | |
| O13 | 0.4318 (3) | 0.7639 (2) | 0.36382 (19) | 0.0115 (4) | |
| O14 | 0.7140 (3) | 0.2355 (2) | 0.27946 (18) | 0.0110 (4) | |
| O15 | 0.1950 (3) | 0.5539 (2) | 0.39618 (18) | 0.0094 (4) | |
| O16 | 0.1507 (3) | 0.3097 (2) | 0.02894 (17) | 0.0112 (4) | |
| O17 | 0.0363 (3) | 0.0833 (2) | 0.14166 (19) | 0.0113 (4) | |
| O18 | 0.6086 (3) | 0.2902 (2) | 0.05605 (18) | 0.0118 (4) | |
| O19 | 0.7564 (3) | 0.4563 (2) | 0.10070 (18) | 0.0104 (4) | |
| O20 | 0.5534 (3) | 0.0239 (2) | 0.3515 (2) | 0.0136 (4) | |
| O21 | 0.0093 (3) | 0.8530 (2) | 0.32331 (17) | 0.0112 (4) | |
| H1 | 0.339 (7) | 0.820 (6) | 0.392 (5) | 0.070 (19)* | |
| H2 | 0.699 (5) | 0.410 (5) | 0.404 (4) | 0.046 (15)* | |
| H3 | 0.440 (5) | 0.069 (6) | 0.328 (5) | 0.060 (17)* | |

*isotropic displacement parameter

(Si), alumina (Al), hematite (Fe), manganese metal (Mn), and magnesium metal (Mg). The $H_2O$ content of the mineral could not be directly measured because of interference with the oxidation of iron and manganese during differential thermal/thermogravimetric (DT-TG) assessments and due to the presence of inclusions; therefore, it was instead calculated based on stoichiometry using the results of Raman spectroscopy and the crystal structure analysis. Total iron was apportioned between FeO and $Fe_2O_3$ based on stoichiometric considerations. The empirical formula, on the basis of 18O + 3OH, is $(Mn^{2+}_{5.36}Mg_{0.27}Fe^{2+}_{0.25}Fe^{3+}_{0.11})_{\Sigma 6.00}(Al_{0.60}Fe^{3+}_{0.40})_{\Sigma 1.00}(Si_{5.89}Al_{0.11})_{\Sigma 6.00}O_{18}(OH)_3$. The ideal formula is $Mn^{2+}_6AlSi_6O_{18}(OH)_3$, which requires $SiO_2$ 41.72, $Al_2O_3$ 5.90, MnO 49.25 and $H_2O$ 3.13, for a total of 100 wt%.

The chemical composition of akatoreite from eastern Otago, New Zealand, is also shown in Table 1 for comparison. The ideal formula for akatoreite is $Mn^{2+}_9Al_2Si_8O_{24}(OH)_8$, which requires $SiO_2$ 37.17, $Al_2O_3$ 7.88, MnO 49.37 and

**Table 5** Anisotropic displacement parameters (Å$^2$) for bunnoite

| | $U^{11}$ | $U^{22}$ | $U^{33}$ | $U^{12}$ | $U^{13}$ | $U^{23}$ |
|---|---|---|---|---|---|---|
| Mn1 | 0.0096 (2) | 0.0102 (2) | 0.0123 (2) | −0.00337 (16) | 0.00200 (16) | −0.00226 (16) |
| Mn2 | 0.0100 (2) | 0.00991 (19) | 0.0096 (2) | −0.00335 (16) | −0.00109 (16) | −0.00204 (15) |
| Mn3 | 0.0097 (2) | 0.00919 (19) | 0.0098 (2) | −0.00373 (16) | 0.00086 (16) | −0.00257 (16) |
| Mn4 | 0.0115 (2) | 0.0135 (2) | 0.0108 (2) | −0.00632 (17) | 0.00276 (16) | −0.00497 (17) |
| Mn5 | 0.0091 (2) | 0.0091 (2) | 0.0091 (2) | −0.00409 (16) | 0.00096 (16) | −0.00217 (16) |
| Mn6 | 0.0089 (2) | 0.0081 (2) | 0.0075 (2) | −0.00359 (17) | 0.00013 (17) | −0.00198 (17) |
| Al7 | 0.0098 (3) | 0.0089 (3) | 0.0104 (3) | −0.0030 (2) | −0.0002 (2) | −0.0033 (2) |
| Si1 | 0.0071 (3) | 0.0066 (3) | 0.0078 (3) | −0.0022 (3) | 0.0008 (3) | −0.0025 (3) |
| Si2 | 0.0062 (3) | 0.0066 (3) | 0.0066 (3) | −0.0021 (3) | 0.0007 (3) | −0.0021 (3) |
| Si3 | 0.0072 (3) | 0.0083 (3) | 0.0068 (3) | −0.0019 (3) | 0.0007 (3) | −0.0022 (3) |
| Si4 | 0.0067 (3) | 0.0073 (3) | 0.0077 (3) | −0.0027 (3) | 0.0009 (3) | −0.0021 (3) |
| Si5 | 0.0068 (3) | 0.0067 (3) | 0.0069 (3) | −0.0024 (3) | 0.0006 (3) | −0.0019 (3) |
| Si6 | 0.0073 (3) | 0.0079 (3) | 0.0086 (3) | −0.0021 (3) | 0.0000 (3) | −0.0030 (3) |
| O1 | 0.0089 (9) | 0.0120 (9) | 0.0119 (10) | −0.0036 (8) | −0.0013 (8) | −0.0023 (8) |
| O2 | 0.0107 (9) | 0.0104 (9) | 0.0080 (9) | −0.0038 (8) | 0.0010 (7) | −0.0034 (7) |
| O3 | 0.0097 (9) | 0.0095 (9) | 0.0135 (10) | −0.0007 (8) | 0.0006 (8) | −0.0050 (8) |
| O4 | 0.0092 (9) | 0.0071 (8) | 0.0113 (10) | −0.0015 (7) | 0.0015 (7) | −0.0031 (7) |
| O5 | 0.0091 (9) | 0.0090 (8) | 0.0106 (9) | −0.0029 (7) | 0.0012 (7) | −0.0033 (7) |
| O6 | 0.0057 (8) | 0.0117 (9) | 0.0105 (9) | −0.0012 (7) | 0.0001 (7) | −0.0048 (7) |
| O7 | 0.0093 (9) | 0.0129 (9) | 0.0122 (10) | −0.0054 (8) | −0.0003 (8) | −0.0022 (8) |
| O8 | 0.0076 (9) | 0.0135 (9) | 0.0117 (10) | −0.0031 (8) | −0.0003 (7) | −0.0057 (8) |
| O9 | 0.0093 (9) | 0.0113 (9) | 0.0123 (10) | −0.0035 (8) | −0.0021 (8) | −0.0019 (8) |
| O10 | 0.0076 (9) | 0.0106 (9) | 0.0110 (9) | −0.0025 (7) | 0.0004 (7) | −0.0036 (7) |
| O11 | 0.0114 (9) | 0.0122 (9) | 0.0068 (9) | −0.0035 (8) | 0.0004 (7) | −0.0026 (7) |
| O12 | 0.0087 (9) | 0.0089 (8) | 0.0106 (9) | −0.0022 (7) | 0.0001 (7) | −0.0040 (7) |
| O13 | 0.0098 (9) | 0.0118 (9) | 0.0139 (10) | −0.0040 (8) | 0.0011 (8) | −0.0055 (8) |
| O14 | 0.0087 (9) | 0.0114 (9) | 0.0098 (9) | −0.0018 (8) | 0.0022 (7) | −0.0019 (7) |
| O15 | 0.0085 (9) | 0.0097 (9) | 0.0098 (9) | −0.0029 (7) | 0.0007 (7) | −0.0035 (7) |
| O16 | 0.0140 (10) | 0.0083 (9) | 0.0085 (9) | −0.0029 (8) | 0.0037 (8) | −0.0012 (7) |
| O17 | 0.0085 (9) | 0.0086 (9) | 0.0176 (10) | −0.0037 (7) | 0.0009 (8) | −0.0046 (8) |
| O18 | 0.0136 (10) | 0.0129 (9) | 0.0121 (10) | −0.0066 (8) | 0.0019 (8) | −0.0062 (8) |
| O19 | 0.0099 (9) | 0.0093 (9) | 0.0132 (10) | −0.0046 (8) | 0.0020 (8) | −0.0043 (7) |
| O20 | 0.0100 (10) | 0.0143 (10) | 0.0199 (11) | −0.0043 (8) | −0.0008 (8) | −0.0092 (8) |
| O21 | 0.0133 (9) | 0.0105 (9) | 0.0088 (9) | −0.0044 (8) | 0.0014 (8) | −0.0021 (7) |

$H_2O$ 5.57, for a total of 100 wt%. Thus, although bunnoite and akatoreite are distinct minerals, their chemical compositions are similar.

## X-ray crystallography

Powder X–ray diffraction (XRD) data for bunnoite were collected using a synchrotron X–ray source on the NE1 beam line of PF–AR, KEK, Japan, which provided a 50 μm diameter collimated beam of monochromatized X–ray radiation (λ = 0.4177 Å). The XRD spectra were collected by the Debye–Scherrer method and recorded using an imaging plate detector, then converted to conventional one-dimensional profiles with the IPAnalyzer and PDindexer software packages (Seto et al. 2010). The resulting data are listed in Table 2. Bunnoite has a triclinic $P\bar{1}$ space group, and the unit cell parameters refined from the powder data are $a$ = 7.521(5) Å, $b$ = 10.008(8) Å, $c$ = 12.048(2) Å, $\alpha$ = 70.46(5)°, $\beta$ = 84.05(6)°, $\gamma$ = 68.31(6)° and $V$ = 793.9(9) Å$^3$.

During additional single crystal XRD assessments, a single crystal of bunnoite was mounted on a glass fiber, and the XRD data were acquired using a Rigaku R–AXIS RAPID curved imaging plate diffractometer with Mo$K\alpha$ radiation monochromatized and focused via a VariMax confocal multilayer mirror. The Rigaku RAPID AUTO software package was used for

**Table 6** Selected bond distances (Å) and angles (°) for bunnoite

| | | | |
|---|---|---|---|
| Mn1-O | | Si1-O | |
| Mn1—O2i | 2.071 (2) | Si1—O18 | 1.588 (2) |
| Mn1—O11 | 2.080 (2) | Si1—O5 | 1.615 (2) |
| Mn1—O1ii | 2.085 (2) | Si1—O14 | 1.650 (2) |
| Mn1—O1i | 2.143 (2) | Si1—O19 | 1.659 (2) |
| Mn1—O14i | 2.438 (2) | <Si1—O> | 1.628 |
| <Mn1—O> | 2.163 | | |
| | | Si2 tetrahedron | |
| Mn2 octahedron | | Si2—O10 | 1.608 (2) |
| Mn2—O9 | 2.039 (2) | Si2—O11 | 1.620 (2) |
| Mn2—O6 | 2.173 (2) | Si2—O16 | 1.627 (2) |
| Mn2—O2i | 2.191 (2) | Si2—O17 | 1.634 (2) |
| Mn2—O11 | 2.238 (2) | <Si1—O> | 1.622 |
| Mn2—O15 | 2.294 (2) | | |
| Mn2—O5 | 2.364 (2) | Si3 tetrahedron | |
| <Mn2—O> | 2.217 | Si3—O2iv | 1.617 (2) |
| | | Si3—O8i | 1.617 (2) |
| Mn3 octahedron | | Si3—O15 | 1.654 (2) |
| Mn3—O18v | 2.099 (2) | Si3—O21 | 1.667 (2) |
| Mn3—O7vi | 2.124 (2) | <Si3—O> | 1.639 |
| Mn3—O10v | 2.188 (2) | | |
| Mn3—O4iv | 2.203 (2) | Si4 tetrahedron | |
| Mn3—O12iv | 2.295 (2) | Si4—O7i | 1.591 (2) |
| Mn3—O10ii | 2.302 (2) | Si4—O4 | 1.622 (2) |
| <Mn3—O> | 1.835 | Si4—O17ix | 1.638 (2) |
| | | Si4—O21 | 1.650 (2) |
| Mn4 octahedron | | <Si4—O> | 1.625 |
| Mn4—O9 | 2.099 (2) | | |
| Mn4—O18vii | 2.143 (2) | Si5 tetrahedron | |
| Mn4—O4 | 2.159 (2) | Si5—O9xi | 1.596 (2) |
| Mn4—O5 | 2.179 (2) | Si5—O12 | 1.607 (2) |
| Mn4—O19vii | 2.327 (2) | Si5—O19 | 1.644 (2) |
| Mn4—O16viii | 2.592 (2) | Si5—O16vii | 1.644 (2) |
| <Mn4—O> | 2.250 | <Si5—O> | 1.623 |
| Mn5 octahedron | | Si6 tetrahedron | |
| Mn5—O7 | 2.078 (2) | Si6—O1 | 1.603 (2) |
| Mn5—O13 | 2.178 (2) | Si6—O6 | 1.605 (2) |
| Mn5—O8 | 2.197 (2) | Si6—O20 | 1.639 (2) |
| Mn5—O12 | 2.199 (2) | Si6—O14 | 1.660 (2) |
| Mn5—O10ix | 2.219 (2) | <Si6—O> | 1.627 |
| Mn5—O20ix | 2.283 (2) | | |
| <Mn5—O> | 2.192 | | |
| | | D—H···A bond | |
| Mn6 octahedron | | O3—H2 | 0.84 (3) |
| Mn6—O13 | 2.126 (2) | O13—H1 | 0.84 (4) |
| Mn6—O4 | 2.142 (2) | O20—H3 | 0.83 (4) |
| Mn6—O5 | 2.145 (2) | H1···O1 | 2.11 (9) |
| Mn6—O12 | 2.169 (2) | H2···O2 | 2.08 (7) |
| Mn6—O3 | 2.172 (2) | H3···O11 | 1.83 (89) |
| Mn6—O15 | 2.244 (2) | O13—H1—O1 | 154.1 (13) |
| <Mn6—O> | 2.166 | O3—H2—O2 | 148.5 (11) |
| | | O20—H3—O11 | 172.5 (13) |
| Al7 octahedron | | | |
| Al7—O6iv | 1.876 (2) | | |
| Al7—O8 | 1.898 (2) | | |
| Al7—O13 | 1.938 (2) | | |
| Al7—O3 | 1.947 (2) | | |
| Al7—O15iv | 1.973 (2) | | |
| Al7—O3iv | 2.113 (2) | | |
| < Al7—O> | 1.958 | | |

processing of the diffraction data, including the application of a numerical absorption correction. he structure was solved by the charge flipping method using Superflip (Palatinus and Chapuis 2007). Based on the symmetries of the electron density distribution calculated by Superflip, the space group $P\overline{1}$ was derived. The SHELXL–97 software package (Sheldrick 2008) was used for structural refinement, employing neutral atom scattering factors. The site occupancies at Si1 to Si6 and Al7 were fixed as 0.98Si + 0.02 Al and 0.60Al + 0.40 Fe based on the chemical analysis. Residual Fe was assigned to the Mn6 site because the ionic radius of $Fe^{2+}$ is smaller than that of $Mn^{2+}$ (e.g., Shanon 1976) and the Mn6 site is the smallest among the regularly coordinated Mn-centered octahedra. Subsequently, the Mn/Mg ratio was refined for the Mn5 and Mn6 sites, which are close in size and have regular octahedral shapes. The Mn1 to Mn4 sites were fixed as 1.0Mn. Moreover, three hydrogen atom positions were identified by difference Fourier syntheses, and these were refined as the locations inferred from neighboring oxygen sites (O3, O13 and O20). The H1, H2 and H3 atoms were bonded to the adjacent O13, O3 and O20 atoms (donors), with the O1, O2 and O13 sites as acceptors. The refined donor-H and H-acceptor distances were approximately 0.85 and 1.8–2.1 Å, respectively, and the donor-H-acceptor angles were around 149–173°. These values are reasonable for an inorganic structure, and the bond valence sums of the atoms are also close to the ideal valence state.

Details of the sample, the data collection process and the structural refinement are provided in Table 3. The final atomic coordinates and equivalent isotropic atomic displacement parameters are summarized in Table 4, while the anisotropic atomic displacement parameters are listed in Table 5. Selected bond lengths and angles are given in Table 6, while the results of bond valence analyses are shown in Table 7. Bunnoite was found to represent a new type of structure, and the structural refinement converged to a final $R1$ index of 3.3 %.

**Table 7** Bond valence analysis for bunnoite

| | Mn1 | Mn2 | Mn3 | Mn4 | Mn5 | Mn6 | Al7 | Si1 | Si2 | Si3 | Si4 | Si5 | Si6 | Total | Ideal |
|---|---|---|---|---|---|---|---|---|---|---|---|---|---|---|---|
| O1 | 0.78 | | | | | | | | | | | | 1.06 | 1.84 | 2 |
| O2 | 0.44 | 0.32 | | | | | | | | 1.02 | | | | 1.77 | 2 |
| O3 | | | | | | 0.32 | 0.80 | | | | | | | 1.12 | 1 |
| O4 | | | 0.31 | 0.34 | | 0.35 | | | | | 1.00 | | | 2.00 | 2 |
| O5 | | 0.20 | | 0.33 | | 0.34 | | 1.02 | | | | | | 1.89 | 2 |
| O6 | | 0.33 | | | | | 0.59 | | | | | | 1.06 | 1.98 | 2 |
| O7 | | | 0.38 | | 0.42 | | | | | | 1.10 | | | 1.90 | 2 |
| O8 | | | | | 0.31 | | 0.56 | | | 1.03 | | | | 1.89 | 2 |
| O9 | | 0.48 | | 0.41 | | | | | | | | 1.09 | | 1.97 | 2 |
| O10 | | | 0.55 | | 0.29 | | | | 1.05 | | | | | 1.89 | 2 |
| O11 | 0.43 | 0.28 | | | | | | | 1.00 | | | | | 1.71 | 2 |
| O12 | | | 0.24 | | 0.30 | 0.32 | | | | | | 1.05 | | 1.91 | 2 |
| O13 | | | | | 0.32 | 0.36 | 0.50 | | | | | | | 1.19 | 1 |
| O14 | 0.16 | | | | | | | 0.92 | | | | | 0.91 | 2.00 | 2 |
| O15 | | 0.24 | | | | 0.26 | 0.46 | | | 0.92 | | | | 1.88 | 2 |
| O16 | | | | 0.11 | | | | | 0.98 | | | 0.96 | | 2.05 | 2 |
| O17 | | | | | | | | | 0.98 | | 0.96 | | | 1.94 | 2 |
| O18 | | | 0.41 | 0.36 | | | | 1.09 | | | | | | 1.86 | 2 |
| O19 | | | | 0.22 | | | | 0.92 | | | | 0.94 | | 2.08 | 2 |
| O20 | | | | | 0.24 | | | | | | | | 0.95 | 1.19 | 1 |
| O21 | | | | | | | | | | 0.88 | 0.94 | | | 1.82 | 2 |
| Total | 1.81 | 1.84 | 1.88 | 1.77 | 1.89 | 1.95 | 2.91 | 3.95 | 4.01 | 3.85 | 4.00 | 4.03 | 3.98 | | |
| Ideal | 2 | 2 | 2 | 2 | 2 | 2 | 3 | 4 | 4 | 4 | 4 | 4 | 4 | | |

## Discussion

The results of the structural analysis are presented graphically in Fig. 4. As shown in the image along the [101] direction, bunnoite has a layered structure consisting of alternating tetrahedral and octahedral sheets parallel to ($\bar{1}$11). In the tetrahedral sheets, there are six unique Si sites, each of which are coordinated to four anions in a tetrahedral arrangement, leading to polymerization of the silicate tetrahedra. Four tetrahedra (Si1, Si2, Si4 and Si5) have two bridging bonds, whereas the Si3 and Si6 tetrahedra each have one bridging bond. In addition, one of the anions in the Si6 tetrahedron (O20) is a hydroxyl ion. These six tetrahedra form a linear [$Si_6O_{18}$(OH)] sorosilicate cluster within the tetrahedral sheet. In the case of the octahedral sheet, there are six unique Mn sites and one unique Al site. Mn1 is coordinated to five oxygen atoms in a pyramidal arrangement, while the base square of the pyramid is distorted with varying bond lengths and angles. Mn4 is coordinated to six oxygen atoms, and the associated octahedron is highly distorted. Other Mn sites (Mn2, Mn3, Mn5 and Mn6) are each coordinated to six anions in an octahedral arrangement, and hydroxyls are included in the Mn5 and Mn6 octahedra. Each Al site is coordinated to four oxygen atoms and two hydroxyl groups in an octahedral arrangement. The octahedra share edges to form continuous strips. Adjacent strips are cross-linked by [$Mn_2O_8$] edge-sharing dimers composted of two Mn1 pyramids which share edges with Mn2 octahedra. The resultant octahedral sheets are connected with tetrahedral sheets by sharing vertices and edges. The edges are shared between the Si5 tetrahedra and Mn4 octahedra and between the Si6 tetrahedra and Mn1 pyramids. The distortions of Mn1 and Mn4 polyhedra are likely a result of edge-sharing with rigid silicate tetrahedra.

To date, six hydrous manganese aluminosilicates have been identified as valid mineral species (Table 8). Among these, structural similarities are evident between bunnoite and akatoreite, although the shape of the unit cells in these minerals is different. Akatoreite was first found in eastern Otago, New Zealand (Read and Reay 1971), and its appearance is shown in Fig. 1 for comparison. The structure of akatoreite was solved by Burns and Hawthorne (1993), and is provided in Fig. 4 for comparison. Both minerals have the same general structural features, consisting of layers of alternating tetrahedral and octahedral sheets, in which silicate tetrahedra make up sorosilicate clusters and the octahedra share edges to form continuous strips linked by polyhedral dimers. However, the polymerized sorosilicate clusters in bunnoite are longer than

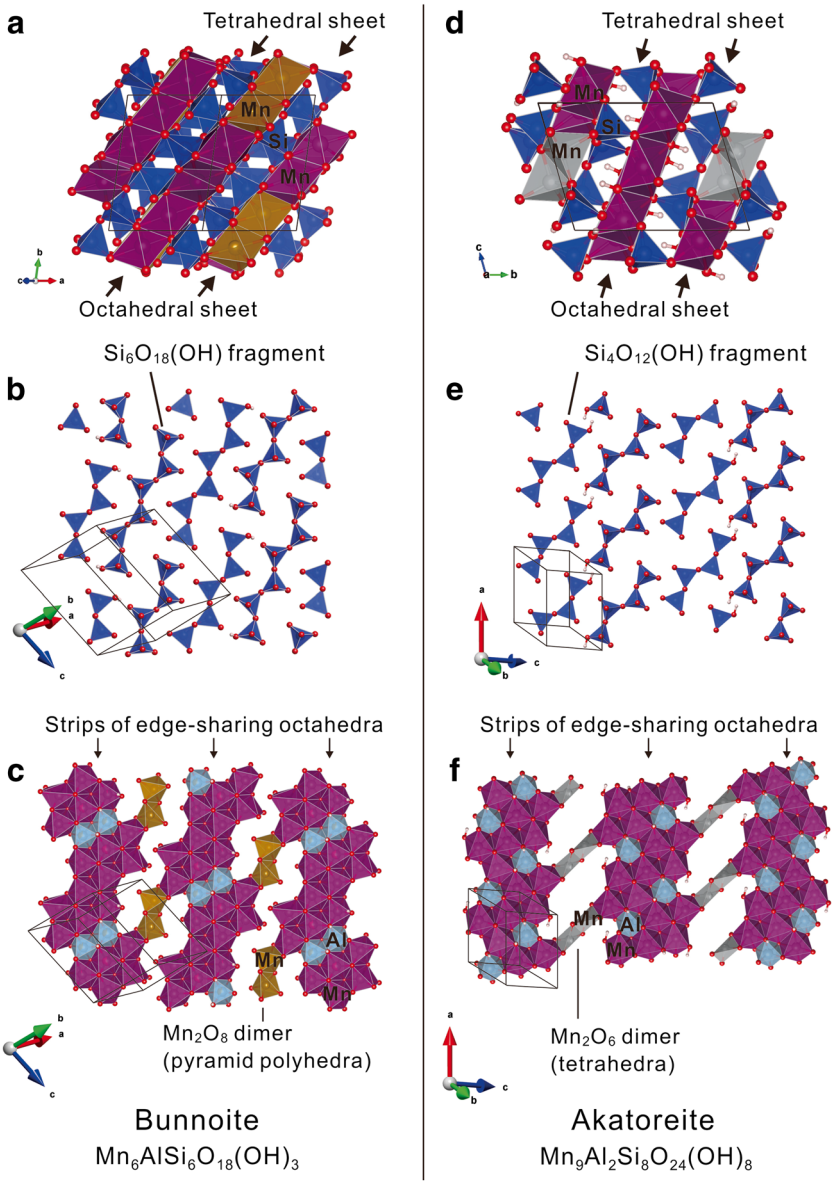


**Fig. 4** The crystal structures of (**a** to **c**) bunnoite and (**d** to **f**) akatoreite. The structures consist of layers of alternating tetrahedral and octahedral sheets, in which silicate tetrahedra make up polymerized sorosilicate clusters and the octahedra share edges to form continuous strips linked by polyhedral dimers. Blue, silicate tetrahedra; grey manganese tetrahedra; light blue, aluminous octahedra; pink, hydrogen; purple, manganese octahedra; ocher, manganese pyramids; red, oxygen

those in akatoreite: $[Si_6O_{18}(OH)]$ in the case of bunnoite and $[Si_4O_{12}(OH)]$ for akatoreite. Bunnoite is the only mineral known to contain $[Si_6O_{18}(OH)]$ clusters. Analogous $[VSi_5O_{18}(OH)]$ clusters have been found in medaite, $Mn^{2+}{}_6V^{5+}Si_5O_{18}(OH)$, and the structure of medaite also consists of layers of alternating tetrahedral and octahedral

**Table 8** Data for hydrous manganese aluminosilicate minerals

| Mineral | Composition | Space group | *a* | *b* | *c* | *α* | *β* | *γ* | Ref. |
|---|---|---|---|---|---|---|---|---|---|
| Akatoreite | $Mn^{2+}{}_9Al_2Si_8O_{24}(OH)_8$ | *P*-1 | 8.337 | 10.367 | 7.629 | 104.46 | 93.81 | 104.18 | 1 |
| Bunnoite | $Mn^{2+}{}_6AlSi_6O_{18}(OH)_3$ | *P*-1 | 7.521 | 10.008 | 12.048 | 70.46 | 84.05 | 68.31 | 2 |
| Carpholite | $Mn^{2+}Al_2Si_2O_6(OH)_4$ | *Ccca* | 13.718 | 20.216 | 5.132 | 90 | 90 | 90 | 3 |
| Davreuxite | $Mn^{2+}Al_6Si_4O_{17}(OH)_2$ | $P2_1/m$ | 9.518 | 5.753 | 12.04 | 90 | 108 | 90 | 4 |
| Kellyite | $(Mn^{2+},Mg,Al)_3(Si,Al)_2O_5(OH)_4$ | $P6_3$ | 5.438 | - | 14.04 | 90 | 90 | 120 | 5 |
| Ottrélite | $Mn^{2+}Al_2O(SiO_4)(OH)_2$ | *Cc* or *C*2/*c* | 9.505 | 5.484 | 18.214 | 90 | 101.46 | 90 | 6 |
| Pennantite | $(Mn^{2+},Al)_6(Si,Al)_4O_{10}(OH)_8$ | *C*-1 or *C*1 | 5.45 | 9.50 | 14.40 | 90 | 97.3 | 90 | 7 |

1; Burns and Hawthorne (1993), 2; This study, 3; Lindemann et al. (1979), 4; Sahl et al. (1984), 5; Peacor et al. (1974), 6; Fransolet (1978), 7; Bayliss (1983)

undulant sheets. Burns and Hawthorne (1993) have suggested that the akatoreite like cluster [$T_4O_{12}$(OH)] is on the border line between the shorter clusters perpendicular to the octahedral sheets and the longer ones that are parallel to the octahedral sheets. The structure consisting of the longer clusters may adapt parallel sheet, and the present case of bunnoite supports their suggestion. Bunnoite contains $MnO_5$ pyramids as the polyhedra having the smallest coordination number, excluding the silicate tetrahedra, so it is classified as 9.BH according to the Nickel-Strunz Classification system.

**Acknowledgments** The authors wish to thank Y. Tamura for acting as a guide at Kamo Mountain. The authors are also grateful to A. Kasatkin for providing a sample of akatoreite. Powder XRD and preliminary single-crystal XRD data were acquired at KEK (Proposal nos. 2013G540, 2014G173 and 2015G522). This work was supported by a Grant-in-Aid for Young Scientists B (Grant No. 15K17785) from the Japan Society for the Promotion of Science.

## References

Bayliss P (1983) Polytypes of pennantite. Can Mineral 21:545–547

Burns PC, Hawthorne FC (1993) Edge–sharing $Mn^{2+}O_4$ tetrahedra in the structure of akatoreite, $Mn^{2+}{}_9Al_2Si_8O_{24}(OH)_8$. Can Mineral 31: 321–329

Fransolet AM (1978) Données nouvelles sur l'ottrélite d'Ottré, belgique. Bull Minéral 101:548–557

Fransolet A, Abraham K, Sahl K (1984) Davreuxite: a reinvestigation. Am Mineral 69:777–782

Lindemann W, Wogerbauer R, Berger P (1979) Die Kristallstruktur von Karpholith $(Mn_{0.97}Mg_{0.08}Fe^{II}{}_{0.07})(Al^{1.90}Fe^{III}{}_{0.01})Si_2O_6(OH)_4$. Neues Jahrb Mineral Monatsh 1979: 282–287

Minakawa T (2000) Akatoreite from iron-manganese deposit of Kamo Mountain in Kurosegawa zone. Abstracts with Programs of Annual Meeting of the Mineralogical Society of Japan, the Mineralogical Society of Japan, P15, 107

Naumova IS, Pobedimskaya EA, Belov NV (1974) Crystal structure of carpholite $MnAl_2(Si_2O_6)(OH)_4$. Kristallografiya 19:1155–1160

Palatinus L, Chapuis G (2007) SUPERFLIP – a computer program for the solution of crystal structures by charge flipping in arbitrary dimensions. J Appl Crystallogr 40:786–790

Peacor DR, Essene EJ, Simmons WB, Bigelow WC (1974) Kellyite, a new Mn-Al member of the serpentine group from Bald Knob, North Carolina, and new data on grovesite. Am Mineral 59:1153–1156

Read PB, Reay A (1971) Akatoreite, a new manganese silicate from eastern Otago, New Zealand. Am Mineral 56:416–426

Sahl K, Jones PG, Sheldrick GM (1984) The crystal structure of davreuxite, MnAl6Si4O17(OH)2. Am Mineral 69:783–787

Seto Y, Nishio-Hamane D, Nagai T, Sata N (2010) Development of a software suite on X-ray diffraction experiments. Rev High Pressure Sci Technol 20:269–276

Shanon RD (1976) Revised effective ionic radii and systematic studies of interatomic distances in halides and chalcogenides. Acta Cryst A32: 751–767

Sheldrick GM (2008) A short history of SHELX. Acta Crystallogr A64: 112–122

Smith WC, Bannister FA, Hey MH (1946) Pennantite, a new manganese-rich chlorite from Benallt mine, Rhiw, Carnarvonshire. Mineral Mag 27:217–220

Wakita K, Miyazaki K, Toshimitsu S, Yokoyama S, Nakagawa M (2006) Geology of the Ino district. Quadrangle Series, 1: 50,000, Geological Survey of Japan, AIST, 140 p